Role of reactive oxygen species in lesion mimic formation, and resistance to F. graminearum in barley lesion mimic mutant 5386

Qunqun Hao
Zaozhuang University
Jifa Zhang
Shandong Agricultural University
Fenxia Guo
Zaozhuang University
Yuhui Wang
Zaozhuang University
Wankun Li
Zaozhuang University
Yindi Di
Zaozhuang University
Fei Ni
Shandong Agricultural University
Daolin Fu
Shandong Agricultural University
Wei Wang (wangw@sdau.edu.cn)
Shandong Agricultural University https://orcid.org/0000-0002-9851-2551
Wenqiang Wang
Zaozhuang University

Research Article

Keywords: Lesion mimic, RNA-Seq, ROS accumulation, antioxidant competence, glutathione, Barley

Posted Date: May 31st, 2022

DOI: https://doi.org/10.21203/rs.3.rs-1642323/v1

Abstract

This study investigated barley lesion mimic mutant (LMM) *5386*, it exhibited a leaf brown spot phenotype and conferred basal resistance to *F. graminearum*. RNA-seq analysis identified 1453 differentially expressed genes in LMM *5368* compared to those in the wild type. GO and KEGG functional annotations suggested that lesion mimic formation was mediated by pathways involving oxidation-reduction and glutathione metabolism. In addition, the accumulation of reactive oxygen species (ROS) in brown spots was substantially higher in LMM *5368*. Antioxidant competence, as indicated by ROS accumulation, was significantly lower in LMM *5368*. Further, the reduction of glycine in LMM *5386* inhibited glutathione biosynthesis. These results suggest that the decrease in antioxidant competence and glutathione caused the accumulation of large amounts of ROS and thus led to programmed cell death in leaves of LMM *5386*, which eventually reduced the yield components in LMM *5386*.

Key Message

LMM *5386* conferred basal resistance to *F. graminearum* and decreased antioxidant competence and GSH content cause ROS accumulation and subsequent PCD.

Introduction

Lesion mimics (LM), also known as hypersensitive reaction-like traits, arise spontaneously in leaf tissue without attack by any plant pathogen (McGrann et al., 2015). Lesion mimic mutants (LMMs) spontaneously form necrotic plaques under normal growth conditions. Thus, LMMs are valuable genetic resources for the study of programmed cell death (PCD) signaling pathways and disease resistance in plants (Moeder and Yoshioka, 2008).

Over the past two decades, many LMMs have been identified and studied in a variety of plants including *Arabidopsis* (Serrano et al., 2010), barley (Hao et al., 2019), maize (Hurni et al., 2015), and rice (Shang et al., 2009). Previous studies of LMM formation have drawn the following conclusions: (1) Mutations or the abnormal expression of disease-resistance genes lead to hypersensitivity and subsequent PCD in plants, causing necrotic plaques similar to those caused by pathogen infection (Shirano et al., 2002); (2) the abnormal expression of genes controlling PCD leads to the loss of control of PCD, which can also lead to the formation of necrotic plaques (Dietrich et al., 1994); (3) plant metabolism disorders can induce necrotic plaques in plants (Hu et al., 1998); and (4) external environmental changes can also induce the appearance of plaques (Wang et al., 2015; Wang et al., 2016). These studies suggest that the pathogenesis of LM is diverse in plants. Therefore, the study of LMMs could elucidate the mechanisms of LM in plants.

To date, very few *Triticeae*-tribe LM genes have been cloned. Two LM genes have been cloned from barley, namely *TIGRINA-D.12* (Khandal et al., 2009) and *NEC1*(Rostoks et al., 2006). *TIGRINA-D.12* and *NEC1* in barley are homologous to *FLU* (At3g14110) and *HLM1* (At5g54250) in *Arabidopsis thaliana*,

respectively. The *FLU* protein regulates chlorophyll synthesis in *Arabidopsis*, and the LMM *FLU* protein forms LM in mature leaves (Meskauskiene et al., 2011). In addition, two LM genes (*lm1* and *lm2*) were mapped on 3BS and 4BL in wheat (Yao et al., 2009). A novel light-dependent LM gene (*lm3*) was mapped on 3BL and showed resistance to powdery mildew in wheat (Wang et al., 2016). However, the current understanding of LMMs is limited; therefore, more LM genes must be identified and studied to illustrate their functions.

LMMs are considered excellent materials for the study of the hypersensitive response (HR) and PCD in plants (Bruggeman et al., 2015). In addition, the level of reactive oxygen species (ROS) has also been identified as capable of producing LMMs (Sindhu et al., 2018). Hao et al. (2019) reported that autonomic lesions associated with *lmm194* were often accompanied by excessive ROS, which occasionally leads to cell death. Plants containing *lmm6* were more resistant to rice blast fungus and had a lower antioxidant competence and higher ROS accumulation (Xiao et al., 2015). Oxidative stress genes are also expressed in LMM individuals (Devadas et al., 2002; Torres et al., 2002), as are enzymes involved in antioxidant systems such as glutathione S-transferase (GST), peroxidase, and superoxide dismutase (SOD) (Klibenstein et al., 1999), suggesting that oxidative stress signals are activated by LMM genes.

Some LMMs have been isolated in plants, most of which display enhanced pathogen resistance. For instance, *lls1* mutant exhibits enhanced resistance to fungal pathogens in maize (Simmons et al., 1998). *spl* mutations exhibited resistance to the blast fungus in rice (Yin et al. 2000). *M66* mutant increased resistance to yellow rust and powdery mildew (Kinane and Jones, 2001). *lm1* and *lm2* enhanced resistance to leaf rust in wheat (Yao et al., 2009), etc.

Barley is both an ideal model of the *Triticeae* tribe and an economically important cereal. In the present study, we identified a novel LMM in barley, and then, we investigated (1) the resistance to *F. graminearum*. and (2) the formation of LM in LMM-containing plants. The results are expected to improve our understanding of the role of LMMs in barley.

Materials And Methods

Plant materials

The experiments were performed at Zaozhuang University, Zaozhuang, Shandong, China. Grains were sown at a density of 300 seeds m^{-2}. The plot size was 2 × 2 m with six rows (0.25 m between rows). Each plot was used for sample collection. The experiments were conducted at least in triplicates.

RNA-seq and data analysis

Flag leaves of WT and LMM *5386* lines were collected, and three biological replicates were used for RNA-seq. Total RNA was extracted from each sample using TRIzol reagent following the manufacturer's specifications (Invitrogen). The quality and quantity of each RNA sample were measured using an Agilent 2100 Bioanalyzer (Agilent Technologies, CA, USA).

The mRNAs were isolated from the total RNA using Dynabeads mRNA DIRECT Kit (Invitrogen) and were separated into short fragments using a fragmentation buffer. Using these short fragments as templates, random primers, and a SuperScript double-stranded cDNA synthesis kit (Invitrogen), double-stranded cDNA was synthesized. Ligated fragments were then generated through a series of reactions that included the purification of the PCR products, end repair, dA-tailing, and ligation of the Illumina adapters. After agarose gel electrophoresis, suitable fragments were selected for PCR amplification. The final library was evaluated using quantitative RT-PCR with a StepOne Plus Real-Time PCR system (Applied Biosystems, Foster City, CA, USA). Sequencing reactions were performed on an Illumina HiSeq 2000 (Biomarker Technologies Corporation, Beijing, China).

GO and KEGG analyses were performed to identify DEGs enriched in GO terms and metabolic pathways, respectively. A corrected p-value (≤ 0.05) was set as the threshold for significantly enriched GO terms and KEGG pathways.

Determination of H_2O_2 content and $O_2\bullet^-$ production rate

H_2O_2 content and $O_2\bullet^-$ production rates were measured according to previously reported methods (Hao et al., 2018). Accumulation of$O_2\bullet^-$ and H_2O_2 in flag leaves was visually evaluated by staining with NBT (0.5 mg mL^{-1}, pH 7.6) for $O_2\bullet^-$ and DAB (1 mg mL^{-1}, pH 3.8) for H_2O_2.

Determination of GSH and Gly content

The GSH and Gly content was measured according to previously reported methods (Noctor et al., 1997).

Measurement of antioxidant enzyme activity

The activities of CAT, SOD, POD, APX, GR, and GST were detected based on previously described methods: SOD (Wang et al., 2020), CAT (Yang et al., 2020), APX (Wang et al., 2017), POD (Wang et al., 2016), GR (Yin et al., 2017), and GST (Li et al., 2018). All samples were analyzed using a Shimadzu UV-1900i spectrophotometer.

Quantitative reverse transcription PCR analysis

Total RNA was isolated from leaves using TRIzol Reagent (Invitrogen, Carlsbad, CA, USA). The RNA was used to produce cDNA using a reverse transcription kit (Vazyme, Nanjing, China). Quantitative reverse transcription PCR was performed using the ChamQ Universal SYBR qPCR Master Mix Kit (Vazyme, China). The expression of a specific gene versus a control was determined using the formula $2^{-\triangle\triangle CT}$. Actin was evaluated as the control gene (Hao et al., 2018). Information on the genes analyzed is presented in Table 2.

Statistical analysis

All analyses were performed at least in triplicate. The IBM SPSS Statistics program was used to perform the statistical analyses. All comparisons were analyzed using factorial ANOVA. Differences between the means among the lines were compared using Duncan's multiple range tests at 0.05 probability levels.

Results

Phenotype analysis of WT and LMM 5368 lines

A barley LMM *5386* line was generated through the application of ethyl methanesulfonate (EMS) to the 'Tamalpais' wild type (WT) cultivar. We found that several brown spots were spontaneously produced in the leaves of LMM *5368* lines under field conditions (Fig. 1a–b). The brown spot area per leaf was quantified in WT and LMM *5368* lines, and that in LMM *5368* lines was significantly higher than in the WT (Fig. 1c).

We also compared the phenotypes of WT and LMM *5368* individuals (Fig. 2a). The tiller number of LMM *5368* was significantly lower (approximately 16.7%) than that of the WT (Fig. 2b), but there were no obvious differences in the plant height (Fig. 2c). Further, the number of leaf brown spots per plant was significantly higher in LMM *5368* plants than that in WT plants (Fig. 1d).

RNA-seq analysis of WT and LMM 5368 lines

To better understand the mechanism of LM formation in LMM lines, we performed an RNA-seq analysis using the flag leaves of WT and LMM *5368* lines. The RNA-seq analysis provided 65.80 Gb of clean bases. The percentage of Q30 in each sample was not less than 93.89%, 91.62–92.09% of reads could be accurately mapped to the reference genome, and 2.38–3.69% of reads could be mapped to multiple genome sequences (Table 1). The Pearson correlation coefficients among biological replicates were found to be higher than 0.95 (Fig. S1).

Compared with WT lines, 1453 differentially expressed genes (DEGs) were found in LMM *5368* lines, of which 1260 were upregulated and 193 were downregulated (Fig. 3). DEGs with the same or similar expression patterns were placed into 16 groups via hierarchical clustering analysis (Fig. S2). For example, the nine DEGs in group 1 were enriched in the glutathione (GSH) metabolic process, GSH transferase activity, anchored component of the plasma membrane, aleurone grain membrane, and cytokinin biosynthetic process (Fig. S3).

The functions of the 1453 DEGs were verified using the gene ontology (GO) database (http://www.geneontology.org), which provides annotations of biological processes, molecular functions, and cellular components. Specifically, we compared the biological process between the WT and LMM *5368* lines. Among the upregulated DEGs, those encoding the protein phosphorylation, oxidation-reduction process, and defense response were clearly over-represented (Fig. 4a). Among the downregulated DEGs, we found that many were significantly enriched in oxidation-reduction and redox homeostasis processes (Fig. 4b).

To compare the metabolic pathways of DEGs in WT and LMM *5368* lines, we analyzed the obtained DEGs using the Kyoto Encyclopedia of Genes and Genomes (KEGG) database (https://www.genome.jp/kegg/pathway.html). Among the upregulated DEGs, many were significantly enriched in GSH metabolism, plant-pathogen interactivity, and amino acid biosynthesis (Fig. 5a). Among the downregulated DEGs, many were significantly enriched in photosynthesis antenna proteins, glyoxylate and dicarboxylate metabolism, and carbon fixation in photosynthetic organisms (Fig. 5b).

ROS analysis of WT and LMM 5368 lines

GO analysis showed that many DEGs were enriched in the oxidation-reduction process (Fig. 4). Therefore, we compared the H_2O_2 content and $O_2{\bullet}^-$ production rate between WT and LMM *5368* lines (Fig. 6). The accumulation of $O_2{\bullet}^-$ was detected via nitroblue tetrazolium (NBT) staining, and $O_2{\bullet}^-$ accumulation in the brown spots of LMM *5368* lines was significantly higher than that in WT plants (Fig. 6a). Similarly, diaminobenzidine (DAB) staining suggested that H_2O_2 content in brown spots of LMM *5368* lines was significantly higher than that in the WT (Fig. 6c). Finally, we quantified the ROS accumulation. As shown in Fig. 6b and d, LMM *5368* lines showed a relatively higher $O_2{\bullet}^-$ production rate and H_2O_2 content than seen in the WT lines.

GSH and glycine (Gly) analysis of WT and LMM 5368 lines

KEGG analysis showed that many upregulated DEGs were significantly enriched in GSH metabolism (Fig. 5a). Therefore, the GSH and Gly content was compared between WT and LMM *5368* lines (Fig. 7a and b, respectively); both were significantly lower in LMM *5368* lines than in the WT.

Antioxidant competence analysis of WT and LMM 5368 lines

Antioxidant enzyme activities were also compared between WT and LMM *5368* lines (Fig. 8). We measured SOD (Fig. 8a), catalase (CAT) (Fig. 8b), ascorbate peroxidase (APX) (Fig. 8c), and peroxidase (POD) (Fig. 8d) activity levels, which were significant in LMM *5368* lines than in the WT. The activities of glutathione reductase (GR; Fig. 8e) and GST (Fig. 8f) were consistent with those of SOD, CAT, APX, and POD. Nevertheless, the downregulation of GR and GST was significantly greater than that of SOD, CAT, APX, and POD in LMM *5368* lines. Further, the antioxidant enzyme-encoding genes of WT and LMM 5368 were compared (Fig. 9). The expression of *Cu/Zn-SOD* (Fig. 9a), *HvCAT1* (Fig. 9b), *HvAPX1* (Fig. 9c), and *HvGST6* (Fig. 9d) genes in LMM *5368* lines were significantly lower than those in the WT.

Resistance to F. graminearum analysis of WT and LMM 5368 lines

RNA-seq analysis indicated that a large number of genes associated with disease resistance were altered between WT and LMM *5368* lines. Therefore, we determined the expression of six disease resistance-related genes, namely, isochorismate synthase (*HvICS*) (Fig. 10a), ethylene response factor 1 (*HvERF1*) (Fig. 10b), *HvWRKY38* (Fig. 10c), pathogenesis related protein-1a (*HvPR1a*) (Fig. 10d), ethylene-responsive transcription factor 3 (*HvERFC3*) (Fig. 10e), and flavonoid O-methyltransferase protein

(*HvFme*) (Fig. 10f). Their expressions in the LMM *5368* lines were up-regulated compared to those in the WT (Fig. 10). We also compared the *F. graminearum* lesions on infected leaves between WT and LMM *5368* lines (Fig. 11). There were no differences in *F. graminearum* lesions at 3DAI between WT and LMM *5368* lines (Fig. 11a, b). After infected with *F. graminearum* at 7d, the length of lesions was significantly larger in all lines. But the lesions in the LMM *5368* were significantly smaller than those in WT (Fig. 11a, b).

Discussion

The brown spots phenotype of LMM 5368 lines

Barley (*Hordeum vulgare*, 2n = 14), the fourth largest cereal crop in the world, offers high yields and good stress tolerance (Hao et al., 2019). Further, barley presents diverse morphological and genetic features and can be used as a model species for the *Triticeae* tribe. In this study, we identified the novel LMM *5386* in barley using EMS (Fig. 1a). LMMs have been classified as “initiation types” and “propagation types” (Landoni et al., 2013). In *LMM* 5386 plants, many brown spots were spontaneously produced at the four-leaf stage and then spread throughout the plant (Fig. 1b; Fig. 2a). Hence, we categorized LMM *5386* as the “propagation type.” However, the mechanism of LM formation remained to be elucidated.

LM caused by ROS accumulation in LMM 5386 lines

RNA-seq is a useful approach for analyzing DEGs at the transcriptome level and in clarifying their regulatory network, thus providing insight into the mechanism of LM formation (Wang et al., 2016). Through transcriptomic analysis, DEG responses were found to be mediated by various pathways (Li et al., 2017), and RNA-seq was used to analyze the 1453 DEGs involved in the formation of LM in LMM *5368* lines (Fig. 3).

PCD can be classified as autolytic and non-autolytic (Van Doorn et al., 2011). Autolytic PCD occurs mainly during plant growth and includes the formation of LM, whereas non-autolytic PCD occurs mainly when plants are subjected to external stress (Van Doorn et al., 2011). ROS such as H_2O_2 and $O_2^{\bullet -}$ are the main participants in the formation and regulation of the HR, which is the most obvious characteristic of PCD (Coll et al., 2011). GO analysis revealed that many DEGs were enriched in the oxidation-reduction process (Fig. 4), suggesting that this process plays an important role in LM formation. In the present study, the accumulation of ROS in brown spots was significantly higher in LMM *5368* lines than in the WT (Fig. 6). Wang et al. (2016) demonstrated that antioxidant enzymes can remove excess ROS to maintain better plant growth. However, the LMM *5368* lines demonstrated lower antioxidant competence, manifested as decreased SOD, CAT, APX, and POD enzyme activities (Fig. 8), which was consistent with the expression of the related antioxidant enzyme-encoding genes (Fig. 9). These results suggest that decreased antioxidant competence leads to the accumulation of ROS and subsequent PCD in LMM *5368* lines.

In rice, many signaling pathways and biological processes are involved in LM and PCD, including protein phosphorylation (Harkenrider et al., 2016), abscisic acid signaling (Wang et al., 2015), and protein ubiquitination (Liu et al., 2015). KEGG analysis showed that many upregulated DEGs were significantly enriched in GSH metabolism (Fig. 5a). H_2O_2 removal is mainly achieved by ascorbate/GSH cycles in higher plants (Noctor et al., 1998), and GSH exists as an intermediate recirculation product in this cycle. GSH is a special class of amino acid derivative consisting of glutamate, cysteine, and Gly. Gly produced by photorespiration plays an important role in GSH synthesis (Noctor et al., 1997). In the present study, we found that Gly content was significantly decreased in LMM *5368* lines, resulting in the inhibition of GSH biosynthesis (Fig. 7). In addition, the decreased activity of GR and GST also reduced the effective clearance of H_2O_2 (Fig. 8e–f), which caused the accumulation of large amounts of ROS and subsequent PCD in LMM *5368* lines. These results suggest that GSH metabolism plays an important role in LM formation.

LMM 5386 **lines showed significant resistance to** F. graminearum

Till now, more than 30 LM mutants exhibiting blast disease resistance have been identified (Zhu et al., 2016), However, there are still few studies on the mechanisms. It was reported that salicylic acid (SA), jasmonic (JA), and ethylene (ET) play an important role in the disease resistance of LM mutants (Kim et al., 2008). we examined *HvICS*, *HvERF1*, *HvWRKY38*, and *HvERFC3*, which encodes a regulator of disease resistance in SA/JA/ET pathways (Lorenzo et al., 2003; Vlot et al., 2009; Hao et al., 2019). In this study, their expressions were significantly increased in the LMM *5368* lines (Fig. 10a, b, c, e). *HvPR1a* and *HvFme* genes, directly involved in disease resistance (Qin et al., 2021), were also significantly up-regulated in the LMM *5368* lines (Fig. 10d, f). Using a leaf-based inoculated *F. graminearum* test, the lesions in the LMM *5368* lines were significantly smaller than those in WT at 7DAI (Fig. 11). The current study proposed that LMM *5368* conferred basal resistance to *F. graminearum*.

In conclusion, the barely LMM *5386*, conferred basal resistance to *F. graminearum* in the present study. The results suggested potential mechanisms of LM formation in LMM *5386*. The decreased antioxidant competence and GSH content cause ROS accumulation and subsequent PCD in LMM *5386*, which eventually reduced the yield components in *LMM 5386* (Table 3).

Declarations

Author contribution statement The work presented here was carried out in collaboration among all authors. WW and WWQ defined the research theme. HQQ and ZJF designed most of the methods and experiments. HQQ, ZJF, GFX, WYH, LWK, and DYD carried out the laboratory experiments. WWQ, NF, and FDL wrote the paper. All authors discussed the results and approved the article.

Acknowledgements This work was supported by the Natural Science Foundation of Shandong (ZR2020QC113), the National Natural Science Foundation of China (32001536), the Science and Technology Plan Projects of Zaozhuang (2019NS01), the Doctoral Research Initiation Funds of

Zaozhuang University (2018BS043, 2020BS001), the Opening Foundation of State Key Laboratory of Crop Biology (2020KF06).

Compliance with ethical standards

Conflict of interest We declare that we do not have any commercial or associative interest that represents a conflict of interest in connection with the work submitted.

References

1. Bruggeman Q, Raynaud C, Benhamed M, Delarue M (2015) To die or not to die? Lessons from lesion mimic mutants. Front Plant Sci 6:24
2. Coll NS, Epple P, Dangl JL (2011) Programmed cell death in the plant immune system. Cell Death Differ 18:1247–1256
3. Devadas SK, Enyedi A, Raina R (2002) The Arabidopsis hrl1 mutation reveals novel overlapping roles for salicylic acid, jasmonic acid and ethylene signalling in cell death and defence against pathogens. Plant J 30:467–480
4. Dietrich RA, Delaney TP, Uknes SJ, Ward ER, Ryals JA, Dangl JL (1994) *Arabidopsis* mutants simulating disease resistance response. Cell 77:565
5. Harkenrider M, Sharma R, Tsao L, Zhang X, Chern M, Canlas P, Zuo S, Ronald PC (2016) Overexpression of rice wall-associated kinase 25 (*OsWAK25*) alters resistance to bacterial and fungal pathogens. PLoS ONE 11:e0147310
6. Hu G, Yalpani N, Briggs SP, Johal GS (1998) A porphyrin pathway impairment is responsible for the phenotype of a dominant disease lesion mimic mutant of maize. Plant Cell 10:1095–1105
7. Hurni SD, Scheuermann SG, Krattinger B, Kessel T, Wicker G, Keller B (2015) The maize disease resistance gene Htn1 against northern corn leaf blight encodes a wall-associated receptor-like kinase. PNAS 112:8780–8785
8. Hao QQ, Lyu B, Tang YH, Wang DY, Li YY, Li QL, Wang YH, Wang WQ (2019) Deterioration of Antioxidant Competence in Barley Lesion Mimic Mutant 194. Phyton-Int J Exp Bot 88:109–117
9. Hao QQ, Wang WQ, Han XL, Wu JZ, Lyu B, Chen FJ, Caplan A, Fu DL (2018) Isochorismate-based salicylic acid biosynthesis confers basal resistance to Fusarium graminearum in barley. Mol Plant Pathol 19:1995–2010
10. Khandal D, Iga S, Frank B, Stephan P, Holger S (2009) Singlet oxygen-dependent translational control in the tigrina-d.12 mutant of barley. PNAS 106:13112–13117
11. Klibenstein DJ, Dietrich RA, Martin AC, Last RL, Dangl JL (1999) LSD1 regulates salicylic acid induction of copper zinc superoxide dismutase in *Arabidopsis thaliana*. Mol Plant microbe In 12:1022–1026
12. Kinane JT, Jones PW (2001) Isolation of wheat mutants with increased resistance to powdery mildew from small induced variant populations. Euphytica 117:251–260

13. Kim KC, Lai Z, Fan B, Chen Z (2008) *Arabidopsis* WRKY38 and WRKY62 transcription factors interact with histone deacetylase 19 in basal defense. Plant Cell 20:2357–2371
14. Liu J, Park CH, He F, Nagano M, Wang M, Bellizzi M, Zhang K, Zeng X, Liu W, Ning Y (2015) The RhoGAP SPIN6 associates with SPL11 and OsRac1 and negatively regulates programmed cell death and innate immunity in rice. PLoS Pathog 11:e1004629
15. Li P, Cao W, Fang H, Xu S, Yin S, Zhang Y, Lin D, Wang J, Chen Y, Xu C (2017) Transcriptomic profiling of the maize (*Zea mays* L.) leaf response to abiotic stresses at the seedling stage. Front Plant Sci 8:290
16. Landoni M, Francesco AD, Bellatti S, Delledonne M, Ferrarini A (2013) A mutation in the FZL gene of Arabidopsis causing alteration in chloroplast morphology results in a lesion mimic phenotype. J Exp Bot 64:4313–4328
17. Li L, Hou MJ, Cao L, Xia Y, Shen ZG, Hu ZB (2018) Glutathione S-transferases modulate Cu tolerance in *Oryza sativa*. Environ Exp Bot 155:313–320
18. Lorenzo O, Piqueras R, Sanchez-Serrano JJ, Solano R (2003) ETHYLENE RESPONSE FACTOR1 integrates signals from ethylene and jasmonate pathways in plant defense. Plant Cell 15:165–178
19. Meskauskiene R, Nater M, Goslings D, Kessler F, Camp R (2011) FLU: a negative regulator of chlorophyll biosynthesis in *Arabidopsis thaliana*. PNAS 98:12826–12831
20. McGrann GR, Burt C, Nicholson P, Brown JK (2015) Differential effects of lesion mimic mutants in barley on disease development by facultative pathogens. J Exp Bot 66:3417–3428
21. Moeder W, Yoshioka K (2008) Lesion mimic mutants: a classical, yet still fundamental approach to study programmed cell death. Plant Signal Behav 3:764–767
22. Noctor G, Arisi ACM, Jouanin L, Valadier MH, Roux Y, Foyer CH (1997) The role of glycine in determining the rate of glutathione synthesis in poplar. Possible implications for glutathione production during stress. Physiol Plant 100:255–263
23. Noctor G, Foyer CH (1998) Ascorbate and Glutathione: Keeping Active Oxygen under Control. Annu Rev Plant Physiol Plant Mol Biol 49:249–279
24. Qin LJ, Tian PD, Cui QY, Hu SP, Jian W, Xie CJ, Yang XY, Shen H (2021) Bacillus circulans GN03 alters the microbiota, promotes cotton seedling growth and disease resistance, and increases the expression of phytohormone synthesis and disease resistance-related genes. Front Plant Sci 12:644597
25. Rostoks N, Deric S, Sharon M, Thomas D, Robert B (2006) Barley necrotic locus nec1 encodes the cyclic nucleotide-gated ion channel 4 homologous to the *Arabidopsis* HLM1. Mol Genet Genomics 275:159–168
26. Simmons C, Hantke S, Grant S, Johal GS, Briggs SP (1998) The maize lethal leaf spot 1 mutant has elevated resistance to fungal infection at the leaf epidermis. Mol Plant Microbe Interact 11:1110–1118
27. Serrano M, Hubert DA, Dangl JL, Schulze-Lefert P, Kombrink E (2010) A chemical screen for suppressors of the avrRpm1-RPM1-dependent hypersensitive cell death response in *Arabidopsis*

thaliana. Planta 231:1013

28. Shang J, Tao Y, Chen X, Zou Y, Lei C, Wang J, Zhu L (2009) Identification of a new rice blast resistance gene, Pid3, by genome-wide comparison of paired nucleotide-binding site–leucine-rich repeat genes and their pseudogene alleles between the two sequenced rice genomes. Genetics 182:1303–1311
29. Shirano Y, Kachroo P, Shah J, Klessig DF (2002) A gain-of-function mutation in an *Arabidopsis* toll interleukin1 receptor-nucleotide binding site-leucine-rich repeat type R gene triggers defense responses and results in enhanced disease resistance. Plant Cell 14:3149–3162
30. Sindhu A, Janick-Buckner D, Buckner B, Gray J, Zehr U, Dilkes BP (2018) Propagation of cell death in dropdead1, a sorghum ortholog of the maize lls1 mutant. PLoS ONE 13:e0201359
31. Torres MA, Dangl JL, Jones JDG (2002) *Arabidopsis* gp91phox homologues AtrbohD and AtrbohF are required for accumulation of reactive oxygen intermediates in the plant defense response. PNAS 99:517–522
32. Van Doorn WG (2011) Classes of programmed cell death in plants, compared to those in animals. J Exp Bot 62:4749–4761
33. Vlot AC, Dempsey DMA, Klessig DF (2009) Salicylic acid, a multifaceted hormone to combat disease. Annu Rev Phytopathol 47:177–206
34. Wang J, Ye B, Yin J, Yuan C, Zhou X, Li W (2015) Characterization and fine mapping of a light-dependent leaf lesion mimic mutant 1 in rice. Plant Physiol Bioch 97:44–51
35. Wang WQ, Hao QQ, Tian FX, Li QX, Wang W The stay green phenotype of wheat mutant *tasg1* is associated with altered cytokinin metabolism.Plant Cell Rep35:585–599
36. Wang WQ, Hao QQ, Wang WL, Li QX, Wang W (2017) The genetic characteristics in cytology and plant physiology of two wheat (Triticum aestivum) near isogenic lines with different freezing tolerances. Plant Cell Rep 36:1801–1814
37. Wang WL, Wang WQ, Wu YZ, Li QX, Zhang GQ, Shi YY, Yang JJ, Wang Y, Wang W (2020) The involvement of wheat U-box E3 ubiquitin ligase *TaPUB1* in salt stress tolerance. J Integr Plant Biol 62:631–651
38. Wang SH, Lim JH, Kim SS, Cho SH, Yoo SC, Koh HJ, Sakuraba Y, Paek NC (2015) Mutation of SPOTTED LEAF3 (SPL3) impairs abscisic acid responsive signalling and delays leaf senescence in rice. J Exp Bot 66:7045–7059
39. Wang F, Wu W, Wang D, Yang W, Sun J, Liu D (2016) Characterization and genetic analysis of a novel light-dependent lesion mimic mutant, *lm3*, showing adult-plant resistance to powdery mildew in common wheat. PLoS ONE 11:e0155358
40. Xiao G, Zhang H, Lu X, Huang R (2015) Characterization and mapping of a novel light-dependent lesion mimic mutant lmm6 in rice (*Oryza sativa* L.). J Integr Agr 14:1687–1696
41. Yao Q, Zhou R, Fu T, Wu W, Zhu Z, Li A, Jia JZ (2009) Characterization and mapping of complementary lesion-mimic genes *lm1* and *lm2* in common wheat. Theor Appl Genet 119:1005–1012

42. Yang JJ, Zhang GQ, An J, Li QX, Chen YH, Zhao XY, Wu JJ, Wang Y, Hao QQ, Wang WQ, Wang W (2020) Expansin gene *TaEXPA2* positively regulates drought tolerance in transgenic wheat (*Triticum aestivum* L.). Plant Sci 298:110596
43. Yin LN, Mano J, Tanaka KS, Wang SW, Zhang MJ, Deng XP, Zhang SQ (2017) High level of reduced glutathione contributes to detoxification of lipid peroxide-derived reactive carbonyl species in transgenic *Arabidopsis* overexpressing glutathione reductase under aluminum stress. Physiol Plant 161:211–223
44. Yin Z, Chen J, Zeng L, Goh M, Leung H, Khush GS, Wang GL (2000) Characterizing rice lesion mimic mutants and identifying a mutant with broad-spectrum resistance to rice blast and bacterial blight. Mol Plant Microbe Interact 13:869–876
45. Zhu X, Yin J, Liang S, Liang R, Zhou X, Chen Z, Zhao W, Wang J, Li W, He M (2016) The multivesicular bodies (MVBs)-localized AAA ATPase LRD6-6 inhibits immunity and cell death likely through regulating MVBs-mediated vesicular trafficking in rice. PLoS Genet 12:e1006311

Tables

Table 1
Summary of the sequence data from RNA sequencing

Samples	Clean reads	Clean bases	GC Content	%≥Q30	Mapped Reads	Multiple Map Reads
5368-1	37,047,360	10,979,042,458	57.65%	94.05%	68,044,432 (91.83%)	1,920,373 (2.59%)
5386-2	37,877,134	11,262,123,100	57.30%	93.89%	69,430,643 (91.65%)	2,093,998 (2.76%)
5386-3	35,801,059	10,557,653,852	57.24%	93.93%	65,598,544 (91.62%)	2,160,694 (3.02%)
WT-1	37,799,868	11,181,592,898	56.97%	94.08%	69,620,925 (92.09%)	2,833,217 (3.75%)
WT-2	37,517,418	11,105,141,892	57.06%	94.04%	69,011,360 (91.97%)	2,040,514 (2.72%)
WT-3	36,100,179	10,713,673,214	57.14%	93.98%	66,411,477 (91.98%)	2,642,342 (3.66%)

Table 2
Primers used in the current study

Target Genes		Primer sequence (5’ – 3’)	Application
HvActin	Forward	TCGCAACTTAGAAGCACTTCCG	qRT-PCR
	Reverse	AAGTACAGTGTCTGGATTGGAGGG	qRT-PCR
Cu/Zn SOD	Forward	CCCCTCACCAAGTCAGTCAT	qRT-PCR
	Reverse	ATTGCAAGTCGGTGTCCTTC	qRT-PCR
HvCAT1	Forward	TGGACGGATGGTACTGAACA	qRT-PCR
	Reverse	GTGCCTTTGGGTATCAGCAT	qRT-PCR
HvAPX1	Forward	CGCCCTCTTGTGGAGAAATA	qRT-PCR
	Reverse	CGCGCATAGTAGCAGCAGTA	qRT-PCR
HvGST6	Forward	ATCTCGTCAGAAACCCGTTC	qRT-PCR
	Reverse	CTTTCCACGACCACACATTG	qRT-PCR
HvICS	Forward	AGATTTACGATGGCGGTTTG	qRT-PCR
	Reverse	TTCAGTGAGCTCGAGGAGGG	qRT-PCR
HvERF1	Forward	GAGGAAGAGCAGAGCGACAC	qRT-PCR
	Reverse	GTCGCCACGAGTATGGTCTT	qRT-PCR
HvWRKY38	Forward	GTGAAGGACGGGTACCAATG	qRT-PCR
	Reverse	GTCGCCACGAGTATGGTCTT	qRT-PCR
HvPR1a	Forward	CACACCAAACCCAGAATGGAGA	qRT-PCR
	Reverse	CGTTGTGGGGTGAAAGGTAGT	qRT-PCR
HvERFC3	Forward	CGTGATGGAGCTTGAGGACCT	qRT-PCR
	Reverse	AGACCGGAGAATCAGATGGAGT	qRT-PCR
HvFme	Forward	TGCTGGTGACATGATGGAGTTC	qRT-PCR
	Reverse	TTACCAGCTTTCTCTCCGTGG	qRT-PCR

Table 3
Yield components of WT and LMM *5386* lines

Cultivar	1000-kernel weight (g)	Spike number	Grain length (mm)	Grain width (mm)
WT	39.5 ± 1.06a	65.0 ± 3.98a	7.03 ± 0.51a	3.07 ± 0.27a
LMM *5386*	37.9 ± 1.13b	64.8 ± 2.45a	6.85 ± 0.47a	2.97 ± 0.22a

Figures

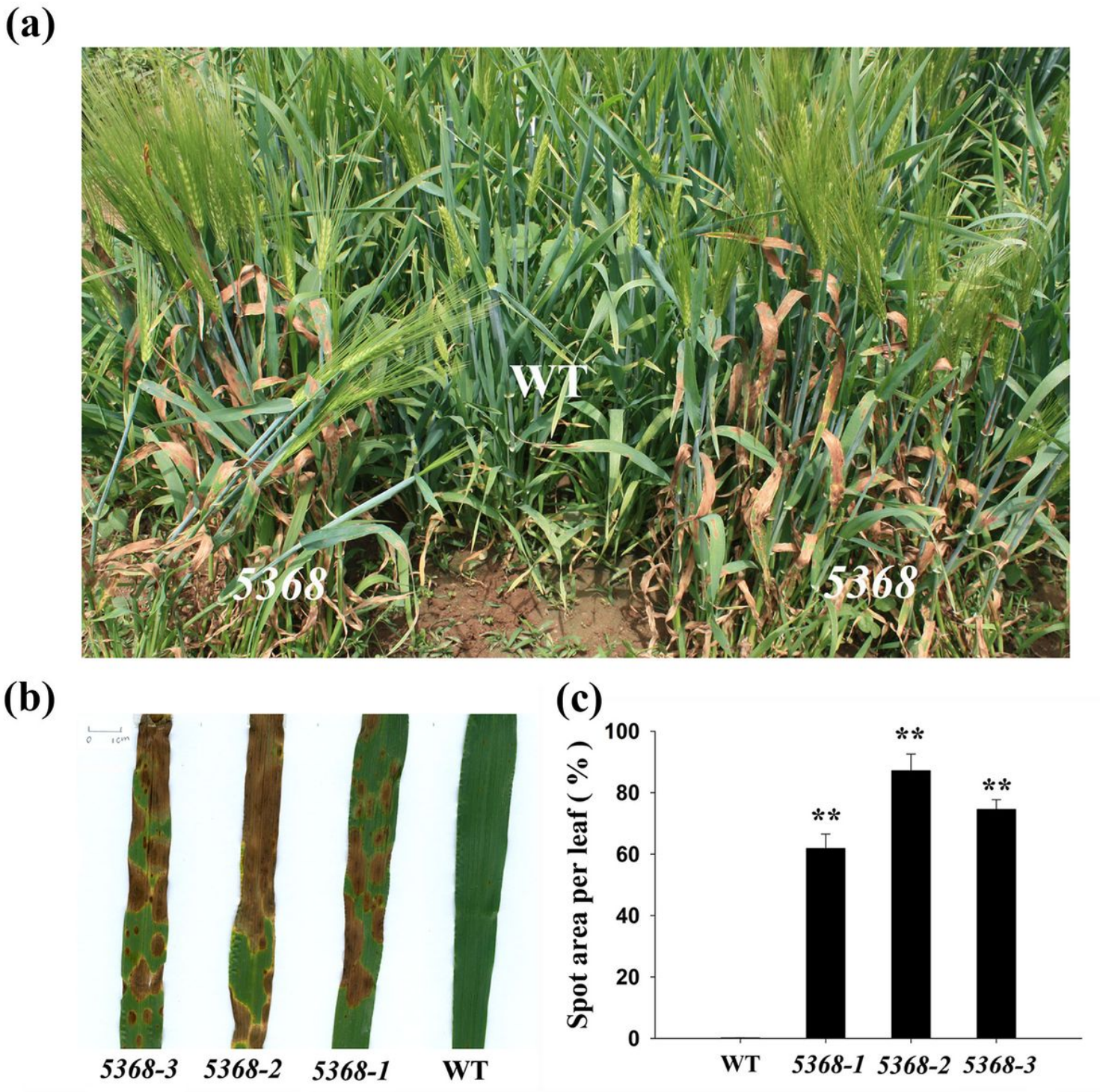

Figure 1

Phenotype differences between WT and LMM *5386* lines in the field. (a) Phenotype in the field; (b) leaf brown spots; (c) spot area per leaf. Values are means ± SD based on 30 replicates. Error bars indicate standard deviations.

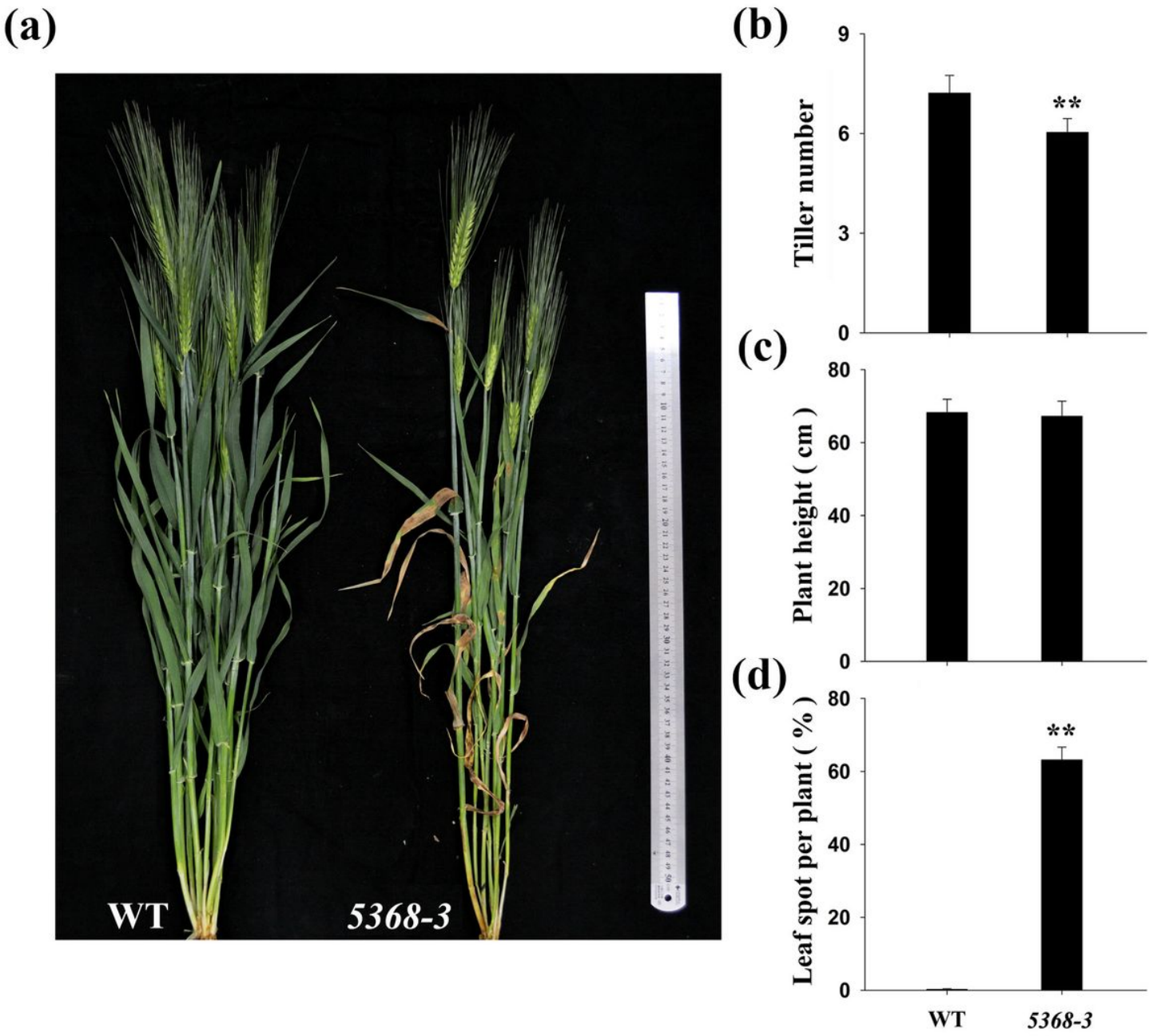

Figure 2

Phenotypes of single WT and LMM *5386* lines. (a) Tiller number; (b) plant height; (c) leaf spots per plant. Values are means ± SD based on 30 replicates. Error bars indicate standard deviations.

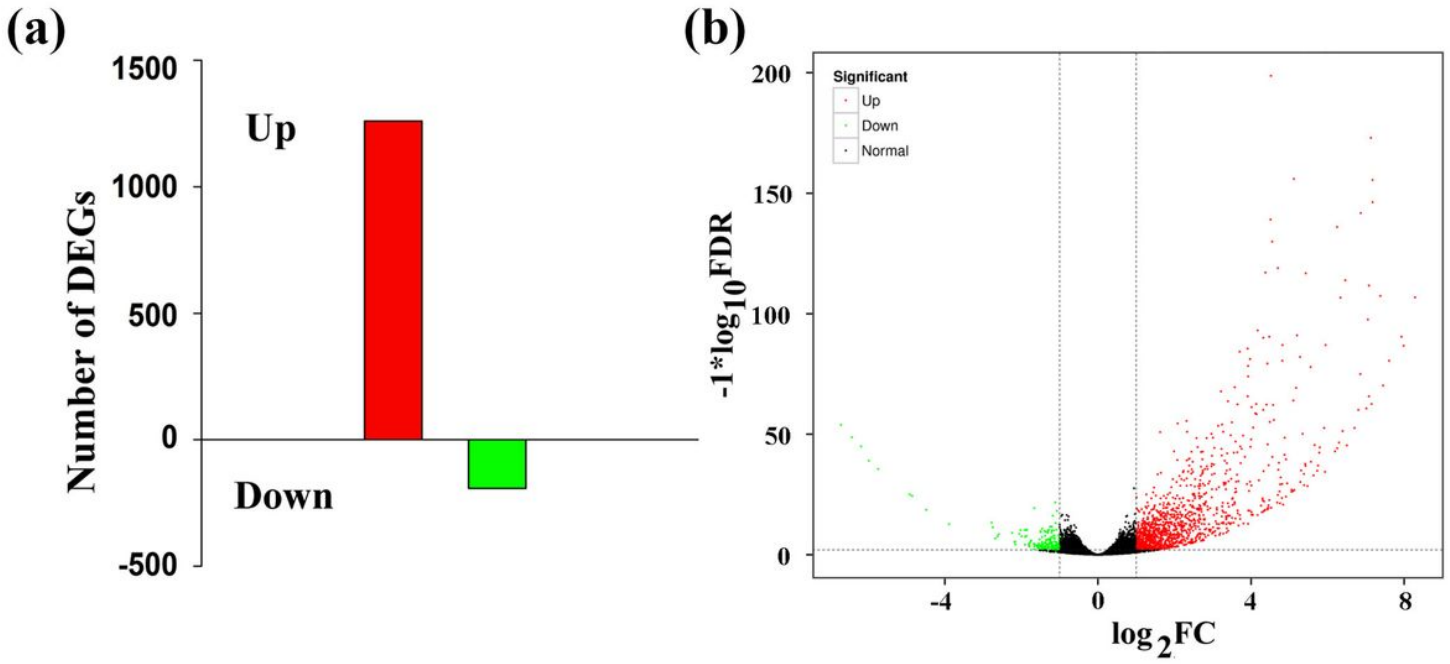

Figure 3

RNA-Seq analysis of WT and LMM *5386*. (a) Changes in the gene expression profiles in WT- and LMM *5386*-line flag leaves; (b) differentially expressed genes (DEGs). Values are means ± SD based on three replicates.

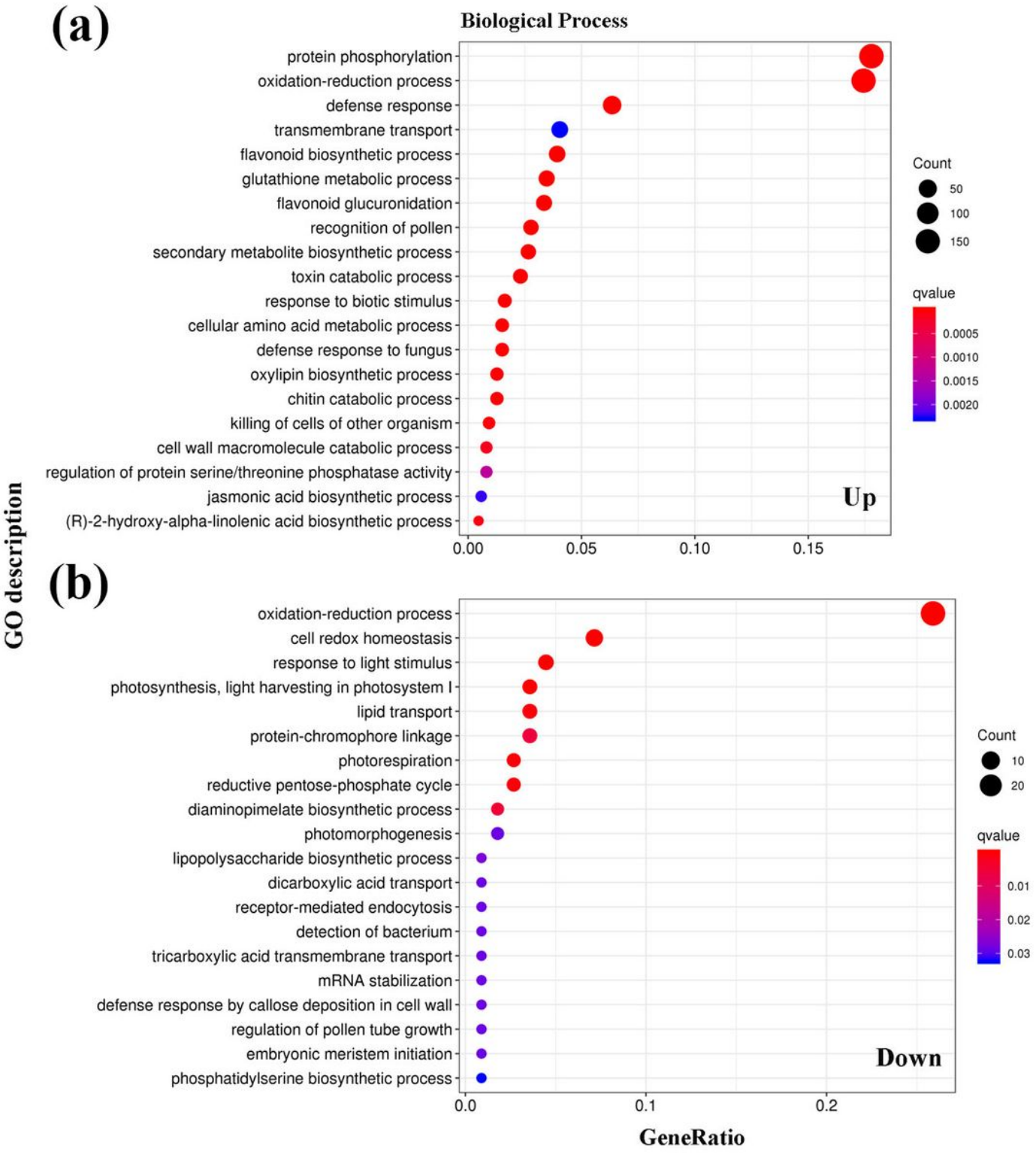

Figure 4

Categories and distribution of Gene Ontology (GO) terms in WT and LMM *5386* lines.

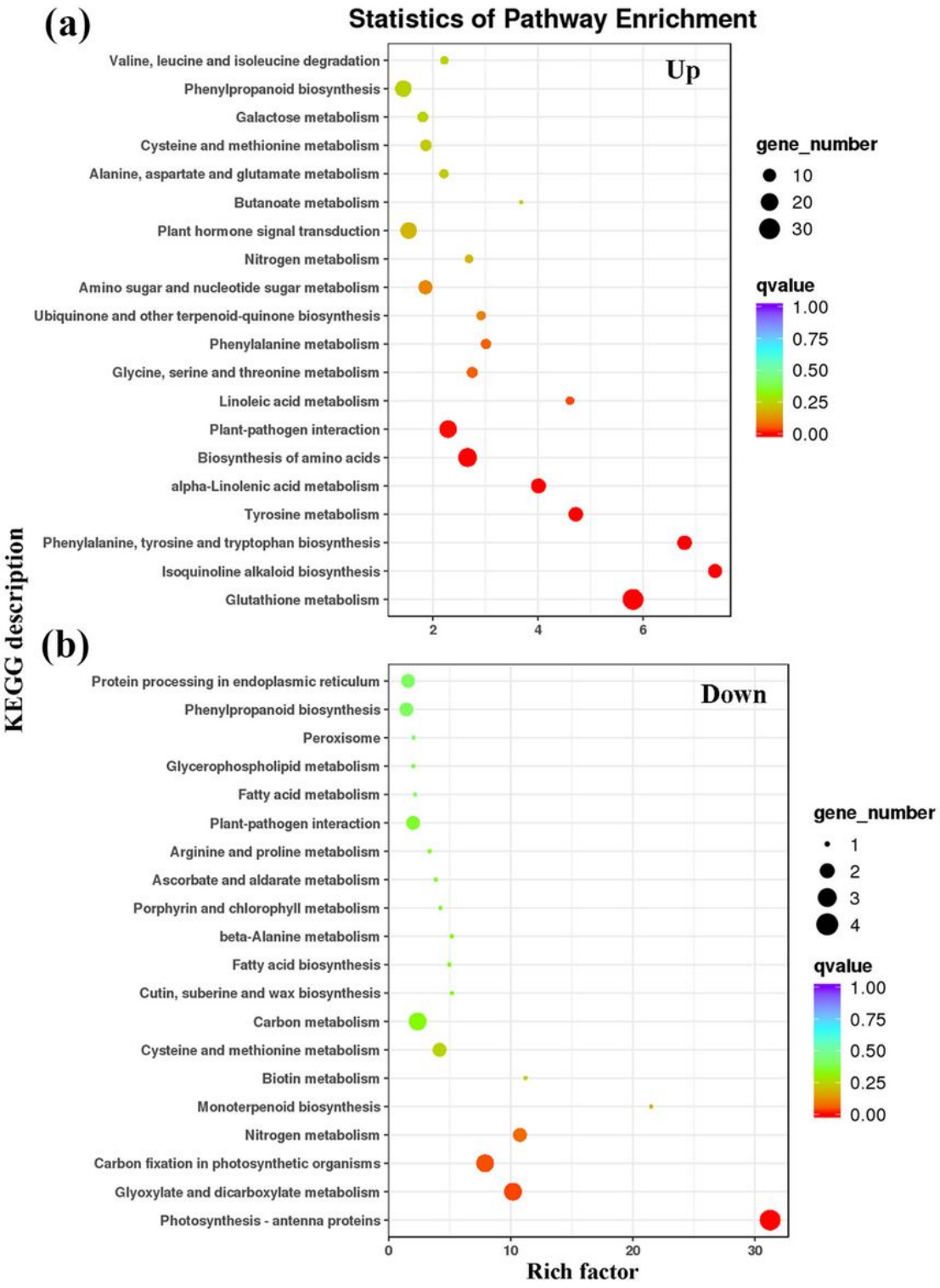

Figure 5

KEGG pathways of prominently enriched differentially expressed genes (DEGs) in WT and LMM *5386* lines.

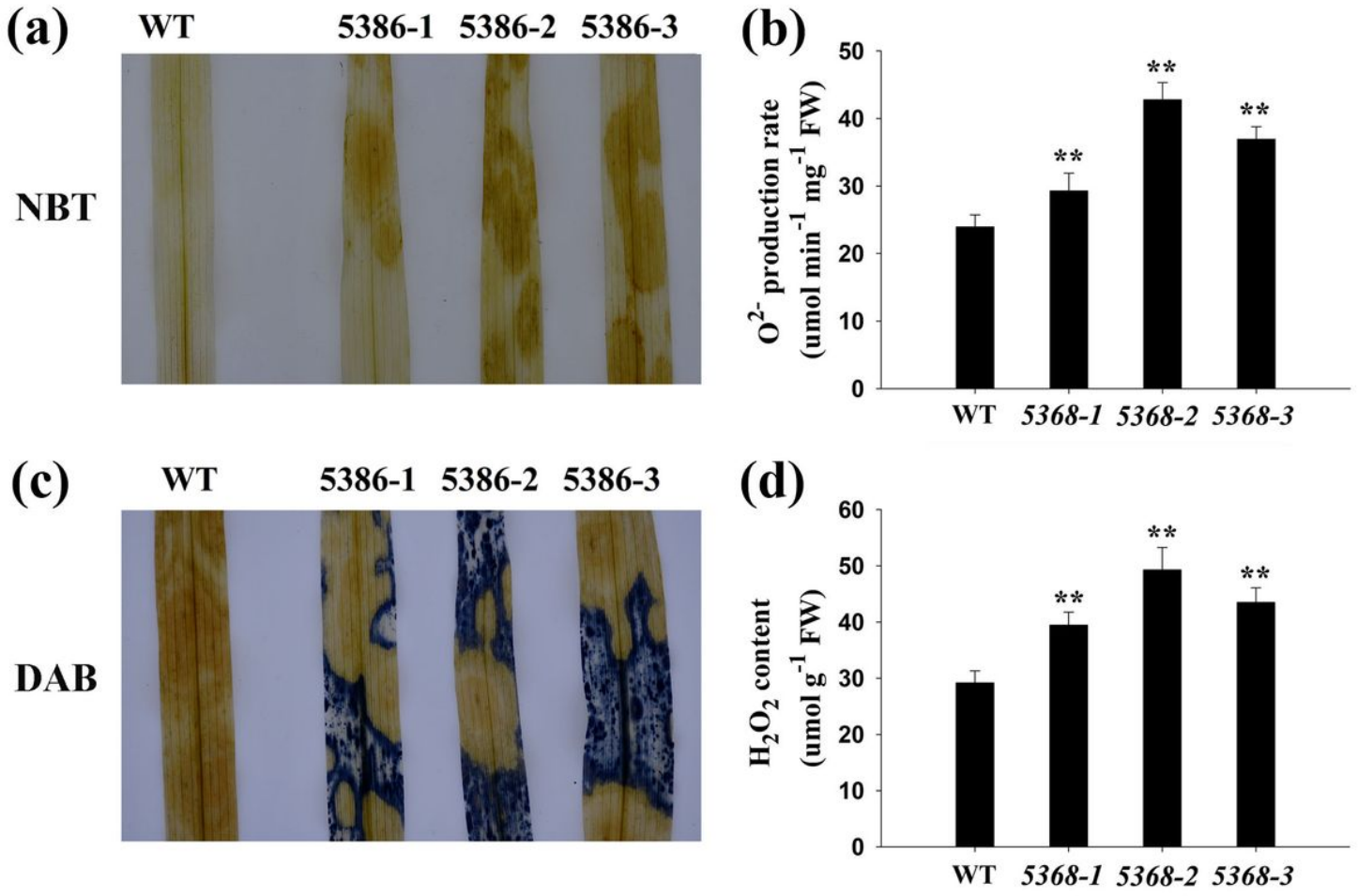

Figure 6

Changes in reactive oxygen species (ROS) accumulation in flag leaves in WT and LMM *5386* lines. (a) NBT staining results for $O_2{\bullet}^-$; (b) $O_2{\bullet}^-$ production rate; (c) DAB staining for H_2O_2; (d) H_2O_2 content. Values are means ± SD of three replicates. Error bars indicate standard deviations.

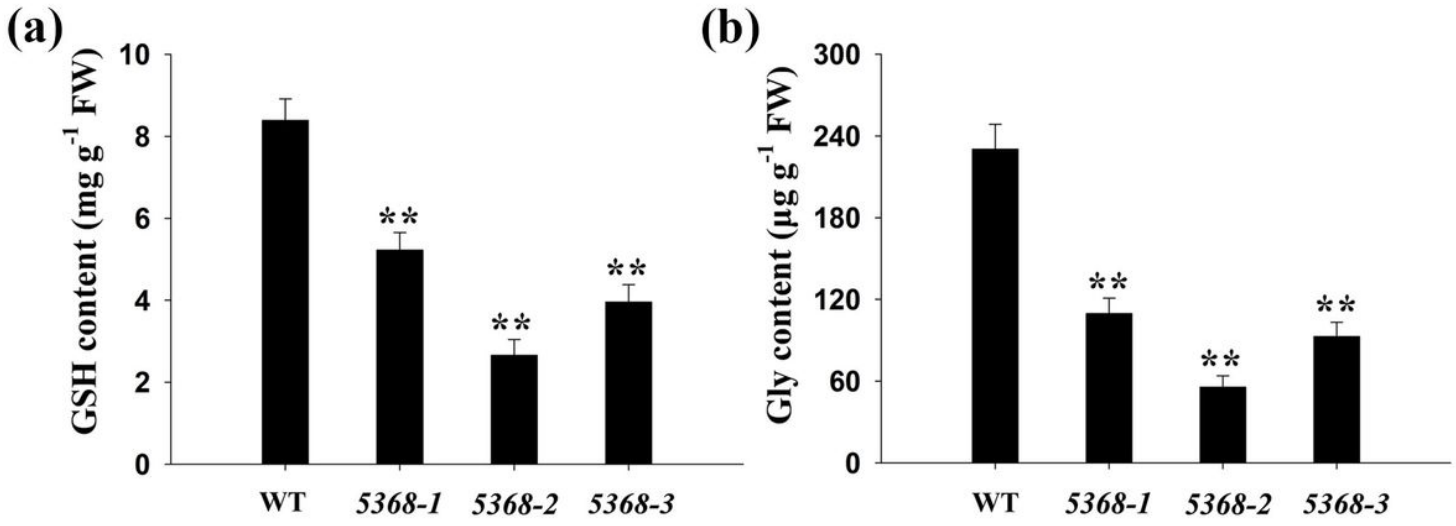

Figure 7

Changes in (a) GSH content and (b) Gly content in flag leaves between WT and LMM *5386* lines. Values are mean ± SD based on three replicates. Error bars indicate standard deviations.

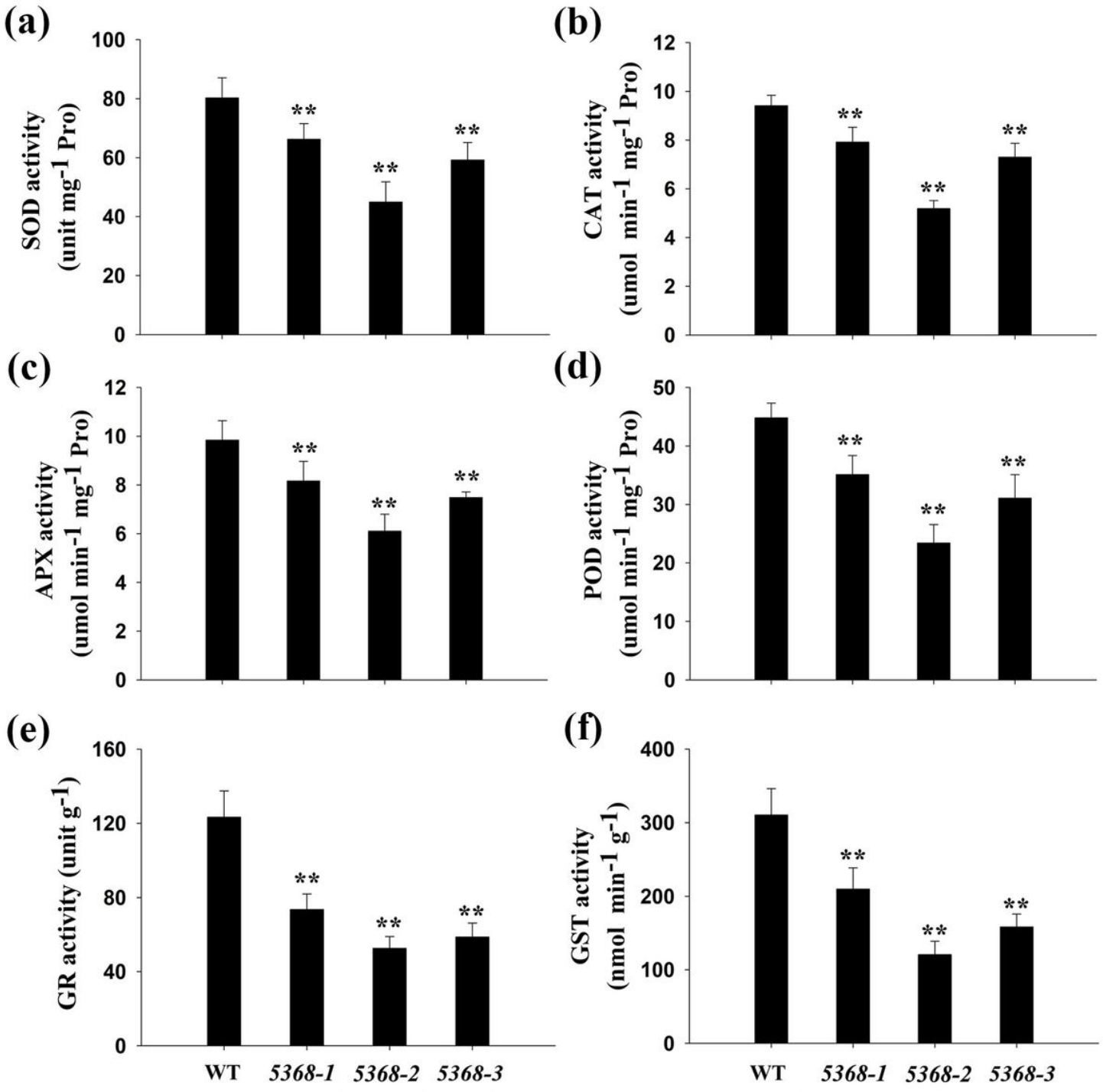

Figure 8

Changes in antioxidant enzyme activity in flag leaves between WT and LMM *5386* lines. (a) Superoxide dismutase (SOD), (b) catalase (CAT), (c) ascorbate peroxidase (APX), (d) peroxidase (POD), (e)

glutathione reductase (GR), and (f) glutathione-S-transferases (GST) activity. Values are means ± SD of three replicates. Error bars indicate standard deviations.

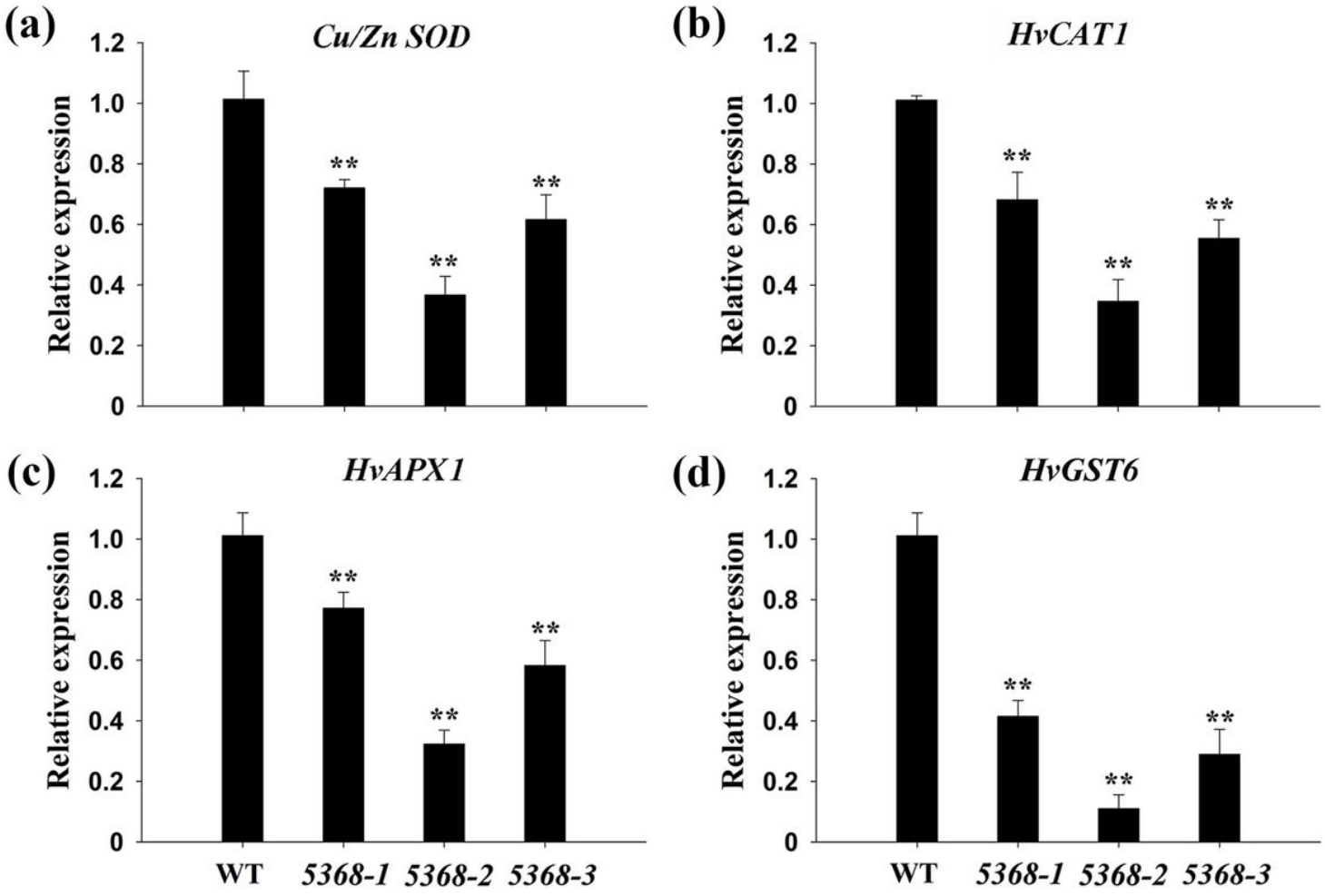

Figure 9

The relative expression of antioxidant enzyme genes in flag leaves of WT and LMM *5386* lines. (a) *C_U/Z_N SOD*, (b) *H_VCAT1*, (c) *H_VAPX1*, and (d) *H_VGST6*. Values are means ± SD based on six replicates. Error bars indicate standard deviations.

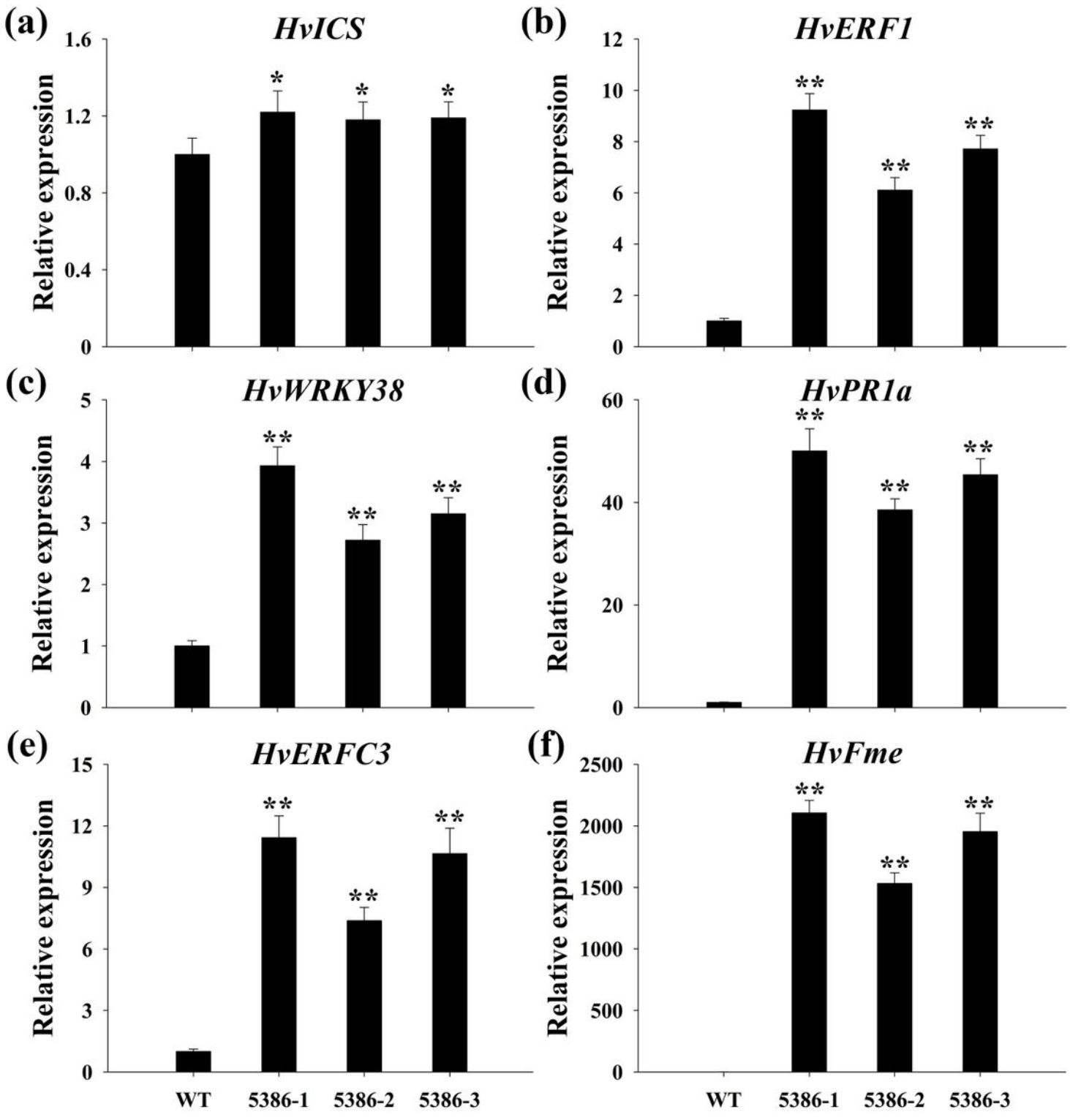

Figure 10

The relative expression of disease resistance-related genes in flag leaves of WT and LMM *5386* lines. (a) *HvICS*, (b) *HvERF1*, (c) *HvWRKY38*, (d) *HvPR1a*, (e) *HvERFC3*, (f) *HvFme*. Values are means ± SD based on six replicates. Error bars indicate standard deviations.

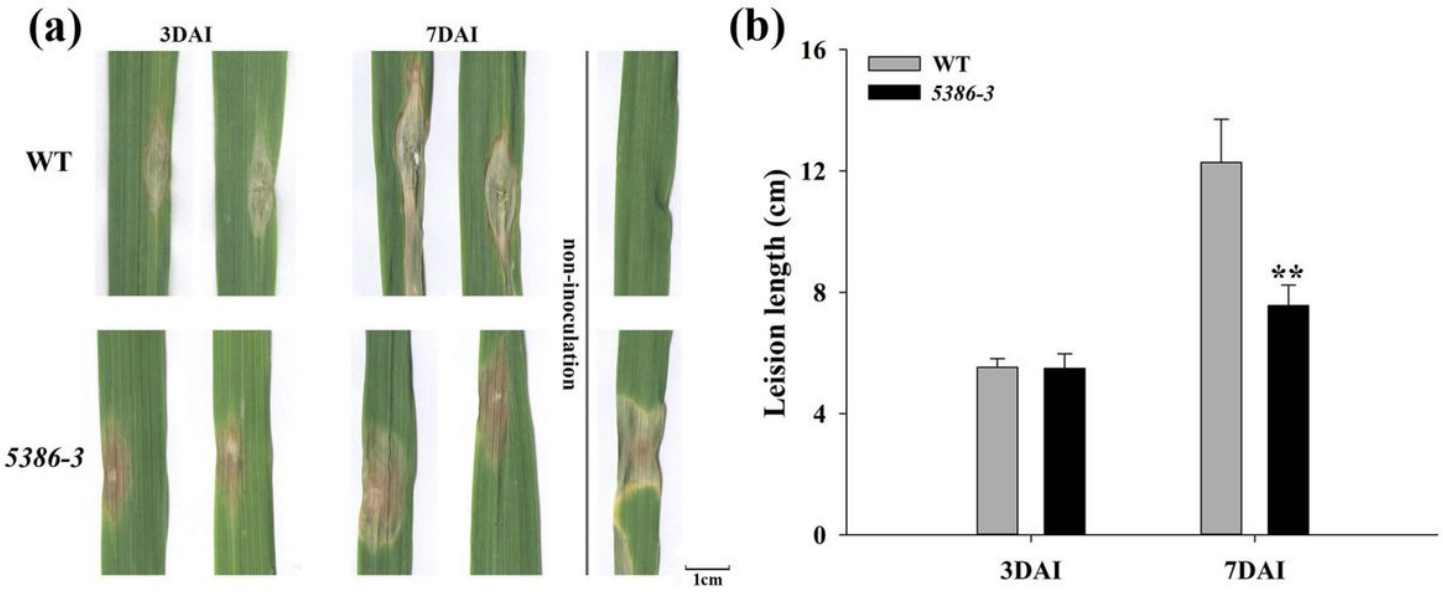

Figure 11

Phenotype differences on inoculated *F. graminearum* in leaves between WT and LMM *5368* lines. (a) Phenotype at 3 days after inoculation (DAI) and 7 days after inoculation (DAI), (b) the leision length. Values are means ± SD based on thirty replicates. Error bars indicate standard deviations.

Supplementary Files

This is a list of supplementary files associated with this preprint. Click to download.

- FigS1.tif
- FigS2.tif
- FigS3.tif